Contents lists available at ScienceDirect

Bioactive Materials

journal homepage: www.keaipublishing.com/en/journals/bioactive-materials

Biomimetic hydrogels with mesoscale collagen architecture for patient-derived tumor organoids culture

Jiaxin Wang [a],[1], Zhilin Sui [a],[1], Wei Huang [b],[c], Zhentao Yu [a],[**], Ling Guo [a],[c],[*]

[a] Shenzhen Key Laboratory of Epigenetics and Precision Medicine for Cancers, National Cancer Center/National Clinical Research Center for Cancer/Cancer Hospital & Shenzhen Hospital, Chinese Academic of Medical Sciences & Peking Union Medical College, Shenzhen, 518116, China
[b] Center for Cell and Gene Circuit Design, CAS Key Laboratory of Quantitative Engineering Biology, Shenzhen Institute of Synthetic Biology, Shenzhen Institutes of Advanced Technology, Chinese Academy of Sciences, Shenzhen, 518055, Guangdong, China
[c] Department of Biology, Academy for Advanced Interdisciplinary Studies, Southern University of Science and Technology, Shenzhen, China

ARTICLE INFO

ABSTRACT

Patient-derived tumor organoids (PDTOs) shows great potential as a preclinical model. However, the current methods for establishing PDTOs primarily focus on modulating local properties, such as sub-micrometer topographies. Nevertheless, they neglect to capture the global millimeter or intermediate mesoscale architecture that have been demonstrated to influence tumor response to therapeutic treatment and tumor progression. In this study, we present a rapid technique for generating collagen bundles with an average length of 90 ± 27 μm and a mean diameter of 5 ± 1.5 μm from tumor tissue debris that underwent mechanical agitation following enzymatic digestion. The collagen bundles were subsequently utilized for the fabrication of biomimetic hydrogels, incorporating microbial transglutaminase (mTG) crosslinked gelatin. These biomimetic hydrogels, referred to as MC-gel, were specifically designed for patient-derived tumor organoids. The lung cancer organoids cultured in MC-gel exhibited larger diameters and higher cell viability compared to those cultured in gels lacking the mesoscale collagen bundle; moreover, their irregular morphology more closely resembled that observed *in vivo*. The MC-gel-based lung cancer organoids effectively replicated the histology and mutational landscapes observed in the original donor patient's tumor tissue. Additionally, these lung cancer organoids showed a remarkable similarity in their gene expression and drug response across different matrices. This recently developed model holds great potential for investigating the occurrence, progression, metastasis, and management of tumors, thereby offering opportunities for personalized medicine and customized treatment options.

1. Introduction

Patient-derived tumor organoids (PDTOs) have emerged as a robust preclinical model that faithfully replicate certain structural and functional aspects of native tumors [1–3]. PDTOs holds immense significance in fundamental biology of oncology, disease modeling, drug discovery, and the advancement of personalized therapies [4,5]. Thanks to advances in the field of material sciences and microtechnology, it is possible to construct microenvironment with different mechanical signals for exploring the influence of extracellular stimulation on organoids growth [6]. Compared to cell lines, PDTO models exhibit both intra- and interpatient tumor heterogeneity [7,8], while also demonstrating significantly lower levels of murine host cell contamination than PDX models [9]. In addition, PDTOs possess the ability to preserve the histological characteristics and gene expression, as well as accurately reflect the drug response of the tumor from which they were derived. Consequently, these models offer a dependable platform for preclinical assessment of anti-cancer drugs and potentially facilitate personalized treatment strategies for cancer patients [1–3]. In recent years, various approaches have been reported for generating PDTO models of different solid tumors, such as colorectal [10,11], lung [1,5], pancreatic [12,13], ovarian [14], prostate [15], breast [6,16,17], and gastric cancers [18].

As a result of these advancements in technology, PDTOs have become an essential instrument for *in vitro* modeling.

Embedment of cells into a solid matrix is crucial for tumor organoids culture. The development of hydrogels that exhibit multi-stimuli (physical, chemical, and biological) responsiveness while closely resembling the natural 3D structure has been extensively documented [19,20]. Recently, increasing focus has been given to the modified gelatin (especially a chemically crosslinked gelatin), which provides reduced variability between batches, a variety of mechanical characteristics, and minimal presence of murine cell contaminants [6,21,22]. The enzymatic crosslinking method has garnered increasing attention owing to its minimal cytotoxicity and gentler reaction conditions [23, 24]. Microbial transglutaminase (mTG) facilitates the formation of hydrogels from gelatin solution by catalyzing the acyltransfer reaction between lysine's 3-amino group and glutamines' g-carboxyamide group in proteins. Additionally, it promotes amide bond transfer within and between protein molecules [23,24]. The enzymatic crosslinking gelatin is used to 3D culture the MSCs and induce their differentiation. It has been previously demonstrated that the gelatin hydrogel crosslinked with mTG demonstrates exceptional capabilities in promoting cell adhesion, proliferation, and differentiation [25–28].

The tissue architecture plays a crucial role in the progression of cancer and how it responds to treatment, regardless of factors such as solid stress, fluid forces, and microenvironment stiffness [29]. The architecture and organization of collagen fibers undergo dynamic alterations during the advancement of tumors [30,31]. Under normal circumstances, the ECM fibers are randomly positioned in an isotropic manner. However, during tumor growth, they adopt a more organized and directional pattern with larger-scale features that significantly influence cellular adhesion, mechanotransduction processes within cells, long-range cell-to-cell communication, and migration [32,33]. The enhanced collagen in the tumor microenvironment undergoes remodeling, resulting in the formation of bundles consisting of collagen fibers that have been linearized and aligned [34,35]. The widths of these bundled collagen fibers within the brain tissue samples obtained from patients diagnosed with glioblastoma multiforme can exceed 2 μm, as observed [36]. Previous investigations into remodeling the tumor ECM *in vitro* have predominantly been concentrated on local properties, including nano-architecture, pore size, collagen alignment or stiffness [37–39]. Typically, these models emphasize sub-micrometer topography and mechanics while lacking mesoscale architectural similarity to the structure of ECM *in vivo*.

Here, we present a methodology for obtaining mesoscale collagen bundles derived from tumor tissue debris that underwent mechanical agitation following enzymatic digestion. Additionally, we combined the mesoscale collagen bundle with mTG crosslinked gelatin to create a composite hydrogel called MC-gel. Biomimetic hydrogels with mesoscale collagen architecture were employed to culture organoids derived from lung cancer patients. The lung cancer organoids (LCOs) grown in MC-gel exhibited larger diameters, higher cell viability, and a more irregular shape compared to those cultured in gels lacking the mesoscale collagen bundle. Furthermore, the LCOs maintained histologic features and mutational landscapes of the parental lung cancer (LC) tissues. The LCOs also exhibited a striking concordance in their gene expression and drug sensitivity across diverse matrices. The findings demonstrate that MC-gel represents an improved option to traditional matrices for the establishment, expansion, and maintenance of PDTOs.

2. Results

2.1. Fabrication and characterization of mTGase gelatin/collagen bundles composite hydrogels

The mesoscale bundled collagen strands, as observed *in vivo* studies, have been consistently associated with tumor progression [32,34–36, 40]. Furthermore, it has been discovered that mesoscale collagen bundles facilitate the adhesion and aggregation of tumor cells (supplementary Fig. 1). In order to fulfill the demand for a precise mesoscale collagen architecture *in vitro* extracellular matrix model, we employed ECM debris to efficiently generate well-defined mesoscale collagen bundles (MCB) with an average length of 90 ± 27 μm and an average diameter of 5 ± 1.5 μm (Fig. 1a–f), which exhibited comparable thickness to those previously reported by the Gong [32] and Liu [33] research group. The ECM debris underwent three cycles of freezing and thawing at −80 °C for decellularization and removal of residual tumor cells from the source tissue. The formation of visible bundles was rapidly induced by mechanical disruption using a high-throughput tissue cell crusher after thawing (Fig. 1a–f).

We chose mTGase crosslinked gelatin hydrogel as co-culture system of mesoscale collagen bundles owe to its good properties in 3D culture [41]. Considering the potential harm to organoids during passage caused by prolonged digestion time, we investigated the impact of mesoscale collagen bundles on the digestion time of mTGase crosslinked gelatin (Fig. 1g–i). The incorporation of mesoscale collagen bundles into mTGase crosslinked gelatin resulted in a significantly reduced digestion time, which was concentration-dependent (Fig. 1i). Furthermore, when MC-gel were treated with either type IV collagenase or Trypsin/EDTA (TE) solution combined with mechanical disruption using a Pipette, MC-gel containing 0.1 % g/ml mesoscale collagen bundles exhibited a remarkably shortened digestion time of approximately 6–8 min, suggesting that utilizing MC-gel for cell passaging eliminates the risk of cell damage caused by prolonged digestion time (Fig. 1g and h).

To test the influence of collagen bundles on gelation time of mTGase gelatin, a bottle-invert test was conducted at 37 °C to measure the MC-gel's gelation speed. The gelation time of MC-gel solution can be fine-tuned by adjusting the dosage of mesoscale collagen bundles. An increase in the dosage of mesoscale collagen bundles resulted in an extended gelation time (Fig. 1j). Furthermore, it was observed that the gelation time showed a direct proportionality with the concentration of mesoscale collagen bundles while maintaining a constant dosage of mTG at 20,000 U/mg pro and a gelatin percentage of 4 % (Fig. 1j). The MC-gel solution, containing less than 0.5 % g/ml of mesoscale collagen bundles, underwent gelation within 20 min, indicating a rapid transition to the gel state. In contrast, when exceeding 0.8 % g/ml of mesoscale collagen bundles in the MC-gel solution, they maintained their fluidic nature and failed to form a hydrogel (Fig. 1j).

We next asked whether the incorporation of mesoscale collagen bundles increase the stiffness of the resultant hydrogel. We found the MC-gel retain constant when the concentration of mesoscale collagen bundles was lower than 0.2 % g/ml. We chose a concentration of 0.1 % g/ml for our subsequent experiments. The Young's modulus of this concentration is 12.56 ± 2.7 kPa (Fig. 1k), which closely aligning with the Young's modulus of lung tumor tissue (12.73 kPa) [42]. This choice ensures the optimal stuffiness and presence of mesoscale collagen architecture observed in the tumor extracellular matrix *in vivo*.

The morphology of the MC-gel and Con-gel was examined through scanning electron microscopy (SEM). The MC-gel displayed a unique and intricate porous structure with smooth pore walls (Fig. 1l). No discernible presence of mesoscale collagen bundles was observed within the scaffold's pore wall, which can be attributed to the good interfacial compatibility between gelatin and mesoscale collagen bundles (Fig. 1l). The pore size of MC-gel was significantly larger compared to that of Con-gel (Fig. 1m). After incorporating mesoscale collagen bundles, the hydrogels exhibited a more prominent three-dimensional network architecture. The frequency sweeps displayed viscoelastic properties in MC-gel, similar to that observed in Con-gel, albeit exhibiting slightly lower frequency-dependent characteristics (supplementary Fig. 2a). The chemical composition of the Con-gel and MC-gel was determined using Fourier transform infrared spectroscopy (FTIR). Both hydrogels exhibited the presence of several similar peaks corresponding to functional groups (supplementary Fig. 2b). The swelling behavior of Con-gel and MC-gel in water exhibits a similar trend, initially experiencing a rapid
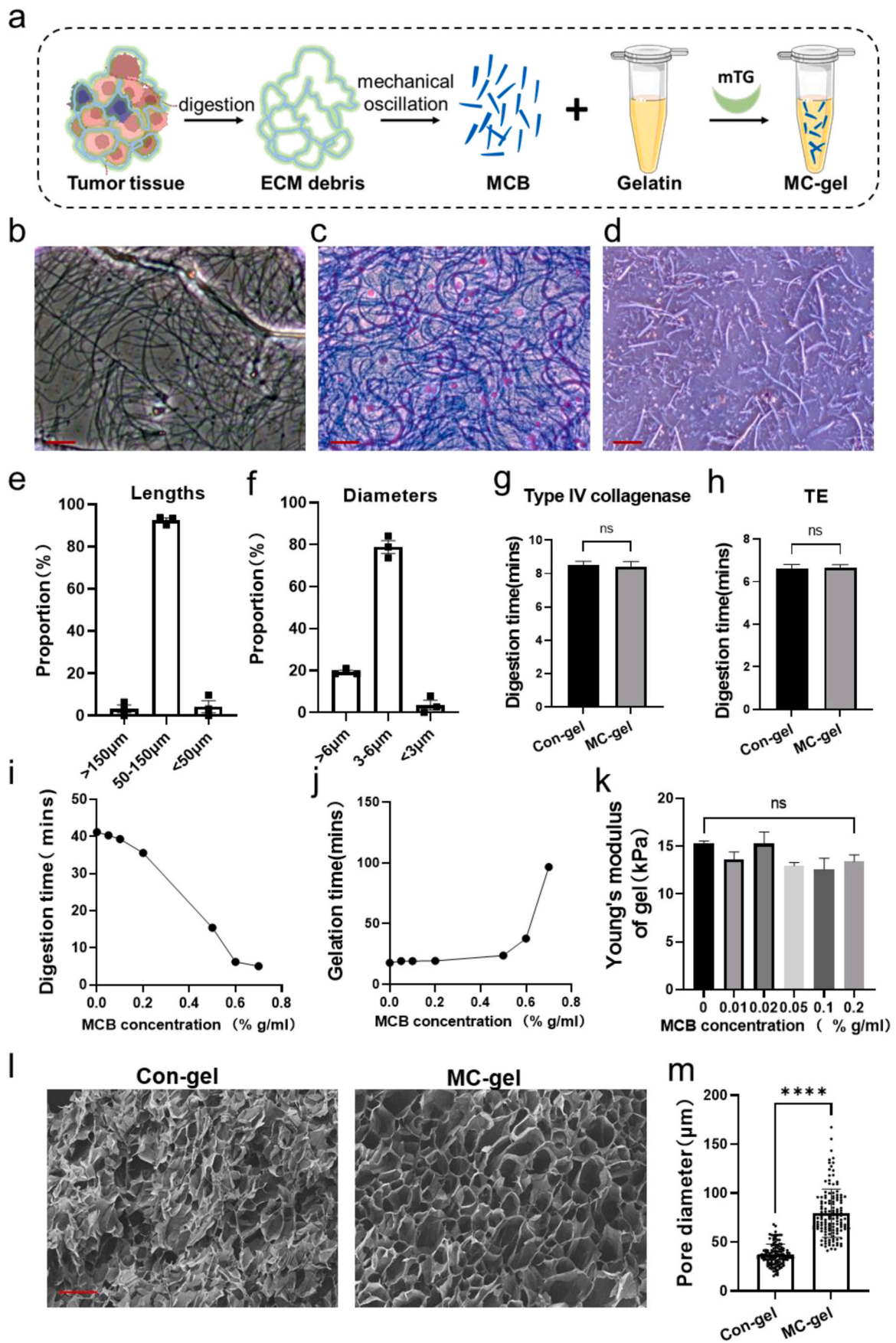
(caption on next page)

Fig. 1. The characterization of composite hydrogels consisting of mTGase crosslinked gelatin/collagen bundles. (a) Schematic diagram of the preparation procedures for MC-gel were shown. MCB refers to mesoscale collagen bundles. (b) Bright-field images of extracellular matrix (ECM) debris were obtained after the removal of residual cells. Scale bar, 100 μm. (c) ECM debris were stained by Masson staining. Scale bar, 100 μm. (d–f) Bright-field images of mesoscale collagen bundle (left, d) were showed and their lengths (e) and diameters (f) were measured. Scale bar, 100 μm. (g–h) The mTGase cross-linked gelatin, containing 0.1 % g/ml of mesoscale collagen bundles (MC-gel) or lacking mesoscale collagen bundles (Con-gel), was fragmented into smaller clusters through trituration using 1 ml pipette tips. Subsequently, it was enzymatically digested either with collagenase IV (g) or TE buffer (h). (i) The digestion time of mTGase cross-linked gelatin with different concentrations of mesoscale collagen bundles. (j) The gelation time of mTGase cross-linked gelatin with mesoscale collagen bundles of different concentrations. (k) The Young's modulus of mTGase cross-linked gelatin with different concentrations of mesoscale collagen bundles was measured at room temperature. (l–m) SEM images of the Con-gel and MC-gel, then the pore diameter was calculated by Image J. Scale bar, 100 μm. The data were reported as the mean ± SD. Data in (e–f), n = 3; data in (i–j), n = 6; data in (k), n = 5; data in (m), n = 130. ****$p < 0.0001$.

increase (supplementary Fig. 2c), eventually reaching equilibrium after 12 h and demonstrating consistent swelling kinetics without any subsequent alterations (supplementary Fig. 2c).

2.2. MC-gel support patient-derived tumor organoid viability and growth

To explore the capabilities of biomimetic hydrogels featuring collagen architecture at a mesoscale level in enhancing the growth and expansion of LCOs derived from primary lung cancer cells, we have effectively cultured 18 organoids sourced from lung cancer cells acquired directly from primary LC tissue. As shown in Table S1. The separation of LC cells was achieved through the integration of mechanical disruption and enzymatic digestion (Fig. 2a). In the presence of mesoscale collagen bundles, LC cells efficiently formed organoids, resulting in a significant 1.3-to-1.8-fold increase in live-cell yields over a 14-day period (Fig. 2b and c); furthermore, these LCOs exhibited a significantly larger diameter compared to those cultured without mesoscale collagen bundle (Fig. 2b). The morphology of LCOs in MC-gel exhibited irregular shapes, which were consistent with the tumor characteristics observed *in vivo*. In contrast, the control group displayed spheroid-shaped organoids (Fig. 2b). Meanwhile, we selected traditional Matrigel (a widely accepted hydrogel for 3D cell culture) and gelatin-added nano-scale collagen (Nano-gel) as control groups. The results demonstrated that LCOs in MC-gel exhibited a higher cell number and larger diameter compared to those in Matrigel and Nano-gel (Fig. 2b and c). Taken together, the data demonstrate that mesoscale collagen architecture promotes tumor multicellular aggregation and organoid growth.

Additionally, we successfully generated mesoscale collagen bundles derived from sarcoma and thyroid cancer samples. Moreover, these two types of tumor organoids were effectively replicated in MC-gel, resulting in a significant increase in cell number and cell diameter compared to those cultured in Con-gel. This clearly demonstrates the potential utility of MC-gel for investigating other solid tumors (supplementary Fig. 3a and b). To emphasize the role of mesoscale collagen in traditional matrices, we incorporated it into Matrigel, a highly regarded hydrogel utilized for three-dimensional cell culture. The inclusion of mesoscale collagen in LCOs within Matrigel resulted in a substantial increase in cell number and larger diameter compared to those without mesoscale collagen (supplementary Fig. 3c).

2.3. LCOs cultured in MC-gel recapitulate the histological features of parental tumors

It is crucial that LCOs cultured in MC-gel adequately retain the histological features of their parental cancer tissue. H&E staining and immunofluorescent staining techniques were employed to compare the morphological and molecular features of LCOs cultured in MC-gel with their parental LC tissues. The LCO-4 derived from lung adenocarcinoma displayed acinar or large glandular patterns, resembling the structure of its parental cancer tissue (Fig. 3a). In addition, consistent expression of molecular markers associated with lung adenocarcinoma, including napsin-A, thyroid transcription factor 1 (TTF-1), and cytokeratin 7 (CK7), and the cell proliferation marker Ki67 was observed in LCO-4 cultivated in MC-gel. This expression pattern closely resembled that seen in its parental LC tissue (Fig. 3b).

Distinct cellular borders and cytoplasmic keratinization were observed in LCO-10 originated from lung squamous cell carcinoma grown in MC-gel, which are commonly seen histological features in tissue affected by squamous cell carcinoma (Fig. 3a). Furthermore, the LCO-10 derived from MC-gel exhibited positive expression of CK5/6 and p63, markers associated with lung squamous cell carcinoma, as well as the proliferation marker Ki67, consistent with their parental lung cancer tissue (Fig. 3c). However, TTF-1 yielded a negative result (Fig. 3c). The cumulative findings demonstrate that tumor organoids cultured in MC-gel accurately replicate the histological characteristics of their parental tumors.

2.4. LCOs cultured in MC-gel preserve the mutational landscape of the original tumors

In order to validate whether the genetic mutations from their parental tumors are retained in different matrixes, Whole exome sequencing (WES) were analyzed on 4 pairs of primary lung cancer tissue and matched LCOs in Con-gel and MC-gel. By implementing germline mutation filtering and applying multiple thresholds, including variant filtering against dbSNP138 and 1000 genomes databases, as well as considering low base quality (<20), low mapping quality (<30), and low variant allele frequency (<0.3), we successfully obtained a set of highly reliable somatic mutations. Somatic mutations in most LC tissues consistently exhibited a high concordance rate ranging 83.3 %–97 % with their corresponding LCOs across the analyzed samples (Fig. 4a). The VAF distribution in the organoids cultured in MC-gel closely resembled that observed in the original LC tissues (Fig. 4b). The sets of four unique LCOs cultivated in the Con-gel and MC-gel exhibited a diverse array of carcinogenic genes, influenced by missense mutations, frameshift mutations, splice site mutations or translation start site mutation, some of which demonstrated variable patterns of alteration. These LCOs within the gels preserved most of the variations present in their original LC tissues, including driver mutations such as TP53 and BCLAF1 (Fig. 4c). We have also detected mutated genes associated with cancer, such as USP8, KEAP1, PTK6, KLF4, PABPC1, PCBP1, and RNF6. It is worth noting that these genetic alterations were highly conserved between LCOs and the original LC tumors (Fig. 4c).

To further assess the degree to which LCO lines maintain their parental tumor's mutation spectrum, we conducted an analysis of somatic mutation patterns in tumor samples and LCOs cultured in different matrices. The basic somatic mutation patterns between LC tissues and corresponding LCOs were well preserved (Fig. 4d). Furthermore, the predominant base substitutions observed in both LC tumor samples and LCOs in MC-gel and Con-gel were C > T/G (Ti) and C > A/G > T transversions (Tv), while T > G/A transversions were found to be the least common mutation type (Fig. 4e), consistent with previously described mutational spectra for lung tumor [43].

2.5. Gene expression profiles exhibit similarity among LCOs cultivated in diverse matrices

The gene expression similarity among LCOs cultivated in diverse matrices was assessed by conducting RNA sequencing of organoids in MC-gel and the corresponding Con-gel. The analysis of gene expression
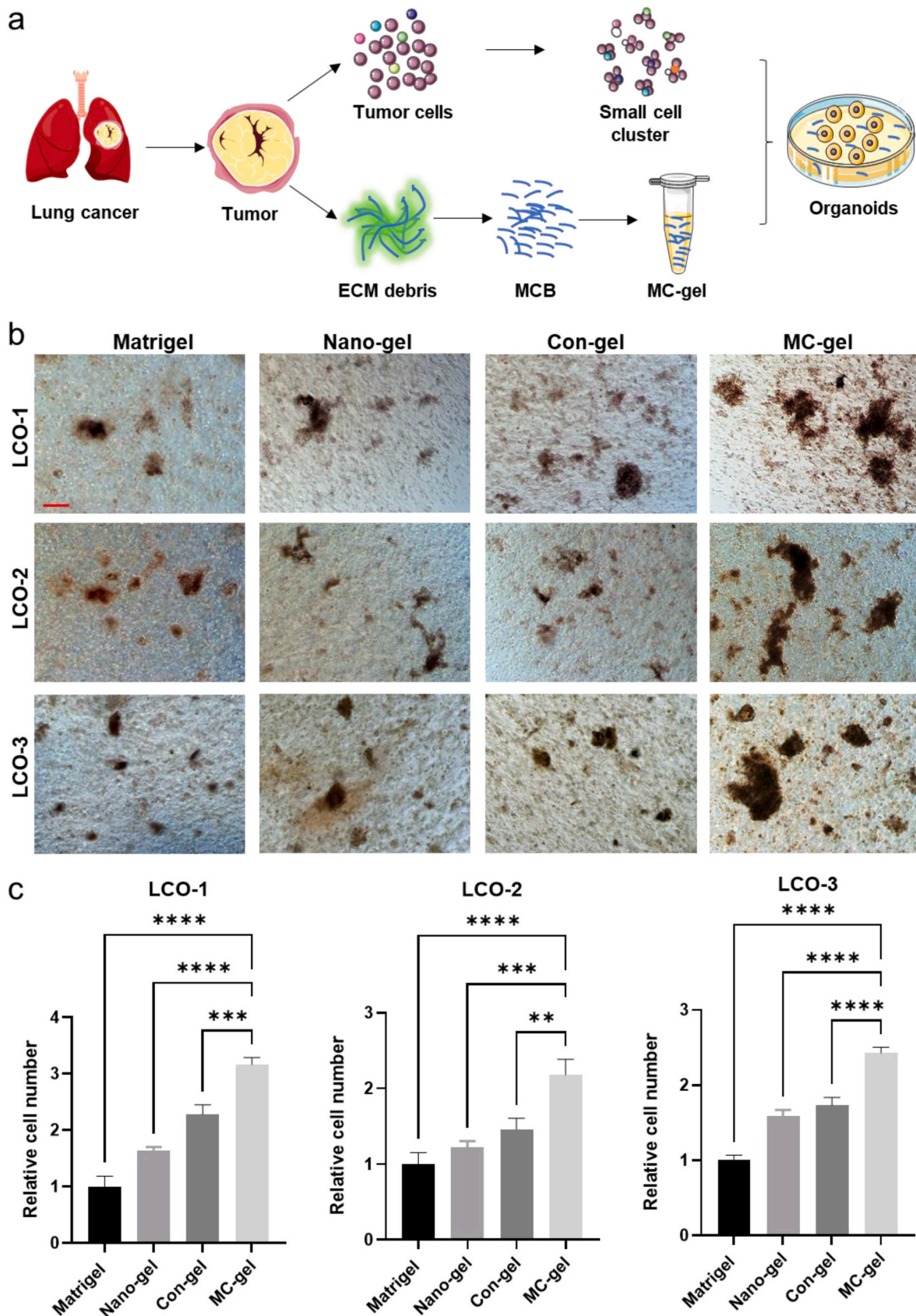
Fig. 2. MC-gel facilitated the growth and propagation of patient-derived LCOs. (a) Schematic representation of the preparation process for patient-derived LCOs. (b–c) The LCOs in the Con-gel, Matrigel, gelatin-added nano-scale collagen (Nano-gel) and MC-gel, were grown for 10–14 days. Representative bright-field images of LCOs were showed and their numbers were measured; Scale bar, 200 μm. Data in (c) were plotted as mean $\pm$ standard deviation (n = 3). **p < 0.01, ***p < 0.001, ****p < 0.0001.
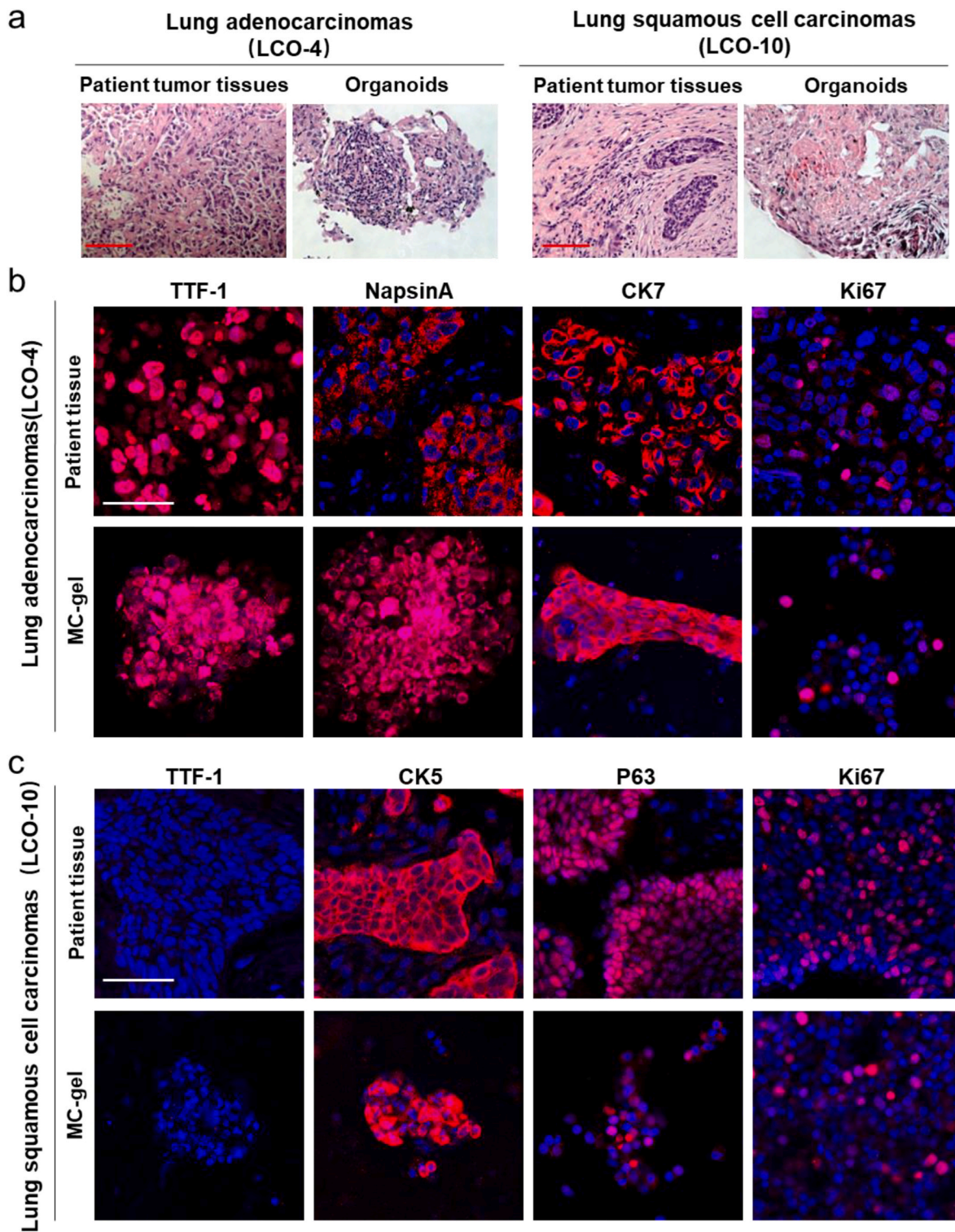
Fig. 3. LCOs cultured in MC-gel recapitulated histopathological characteristics of parental tumors. (a) The H&E-stained images of LCOs and their corresponding LC tissues were presented. Scale bar, 100 μm. (b) The LCO-4 derived from lung adenocarcinoma in the MC-gel, as well as their corresponding parental tumor tissues, were acquired for immunofluorescence analysis of TTF-1, Napsin A, CK7, and Ki67. DAPI (blue) was used to stain the nuclear. (c) The LCO-10 in MC-gel, as well as their corresponding parental tumor tissues, derived from a lung squamous cell carcinoma sample, were subjected to immunofluorescence staining for TTF-1, p63, CK5/6, and Ki67. Representative images of immunofluorescence were presented. Scale bar, 50 μm.

correlation revealed a highly concordant expression profile in each LCO line cultured in MC-gel and its corresponding Con-gel. Moreover, the overall gene expression correlation between MC-gel and Con-gel for the LCO exceeded 0.948. (Fig. 5a). Furthermore, the application of principal components analysis (PCA) facilitates enhanced visualization of more

subtle variations. The principal component analysis (PCA) results of four LCO lines cultured in MC-gel and its Con-gel were presented in Fig. 5b. In the case of LCO-5,7,8,9 lines cultured in MC-gel and their respective Con-gel, there was a tendency for clustering. The LCO-7 and LCO-9 lines in the MC-gel exhibited a relatively close association with those in the
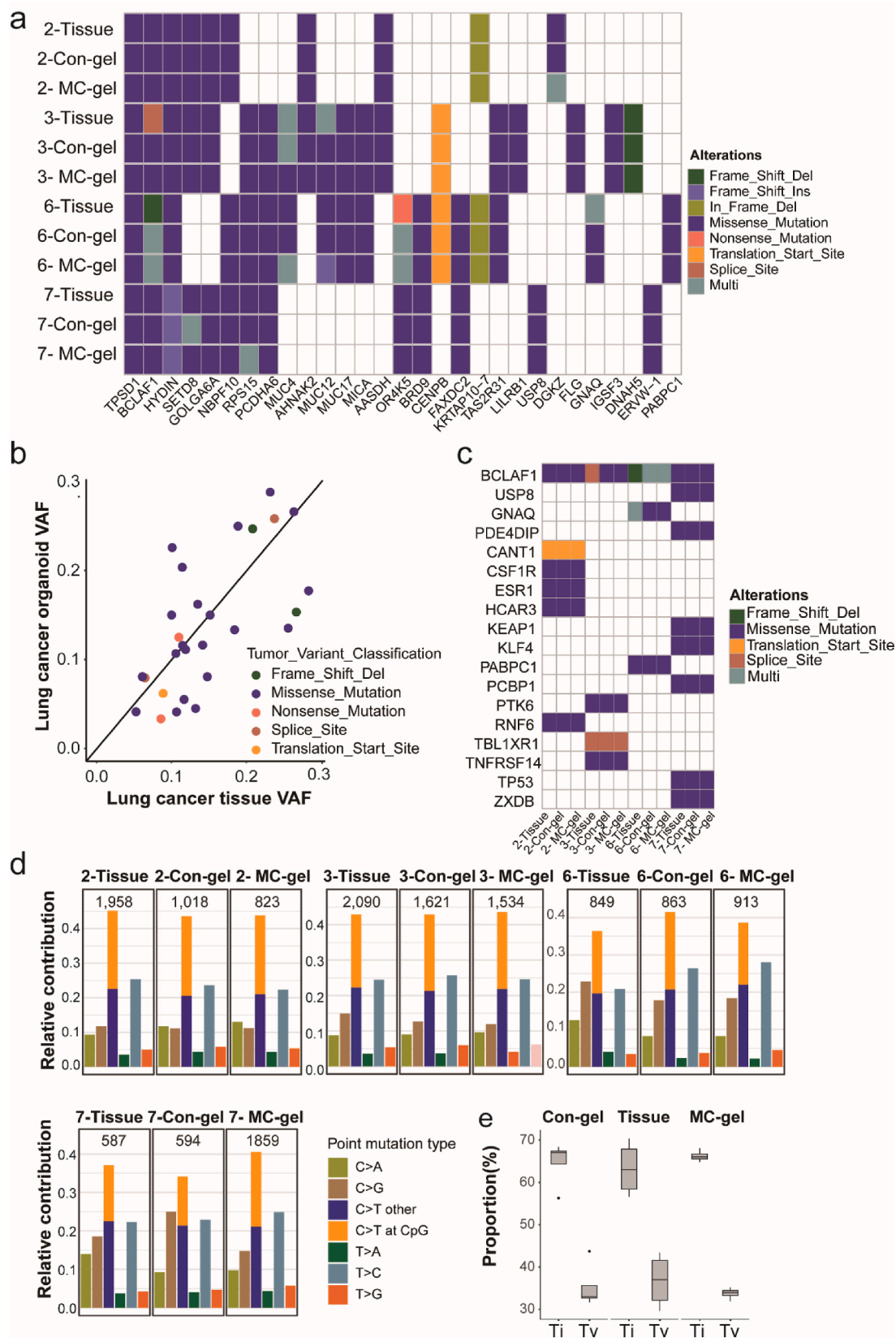
Fig. 4. LCOs cultured in MC-gel retained the genetic characteristics of the original tissues. (a) Heat-map analysis was conducted on the top 30 mutations in LCOs cultured in Con-gel and MC-gel and their corresponding LC tissues. (b) The VAF of genetic alterations detected in LCOs in MC-gel was compared with that of their parental LC tissues (c) Heatmap visualizing somatic mutations that impact cancer genes in LC tissues and their corresponding LCOs in Con-gel and MC-gel conditions. (d) The proportions of exonic variants in LCOs in Con-gel and MC-gel, as well as their parental tumors, were presented. Additionally, the legend provided information on the seven distinct types of base substitutions. The numbers at the top of the figures depicted the amounts of mutations. (e) Percentage of Ti and Tv transversions of three groups were shown.
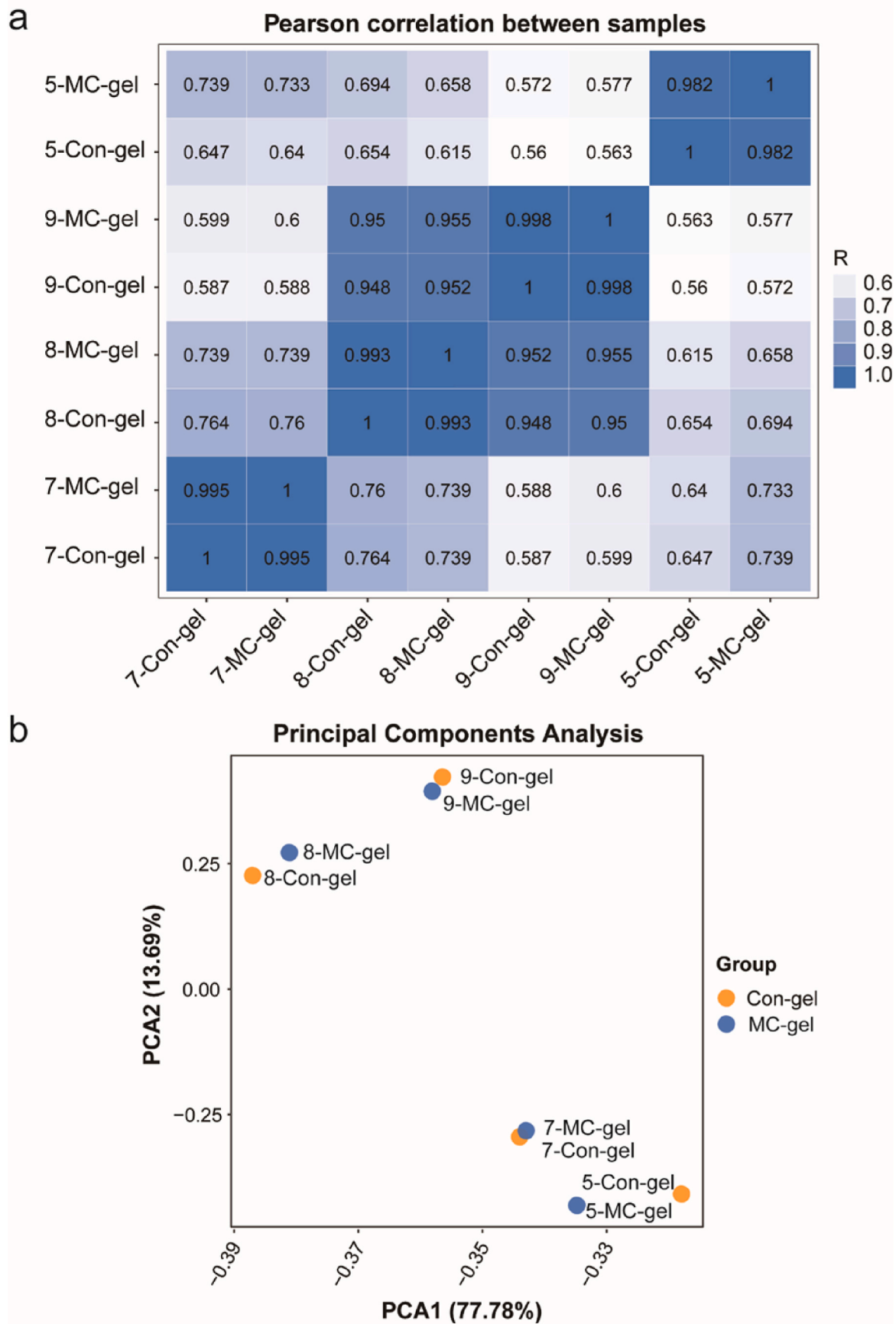
Fig. 5. Gene expression of LCOs in Con-gel and MC-gel. (a) Correlation heatmap of LCOs grown in Con-gel and MC-gel based on RNA-seq data. (b) The RNA-seq data of LCOs cultured in different matrices was subjected to Principal Components Analysis (PCA).

Con-gel, while there was a slight disparity between the control and MC-treated organoids for LCO-5 and LCO-8 as observed in the PCA scores plot. The RNA expression data overall suggest that MC-gel enables organoid tumor cells to largely preserve the RNA expression properties observed in their Con-gel.

2.6. LCOs cultured in MC-gel maintain drug sensitivity

We subsequently evaluated the feasibility of utilizing six LCO lines cultured in MC-gel for conducting drug sensitivity assays. The LCO lines cultivated in MC-gel and Con-gel were subjected to a panel of drugs commonly administered for lung cancer therapy: doxorubicin, cisplatin, erlotinib, and paclitaxel (Table S2). After an incubation period lasting from 7 to 10 days, the tumor organoids were subsequently subjected to a drug treatment lasting for 3–5 days. Following completion of this drug treatment, the cell viability was assessed. The sensitivity of each LCO

lines were determined by performing technical replicates using a panel of four anti-cancer drugs (Fig. 6a). Drug sensitivity was measured based on relative cell survival.

The LCOs in the Con-gel and MC-gel exhibited a consistent trend for each drug, indicating that the presence of mesoscale collagen bundle did not significantly impact chemotherapy sensitivity across most organoid cultures (Fig. 6b). Meanwhile, The LCOs derived from different patients, both in the Con-gel and MC-gel, exhibited significant variations in their responses to the four chemotherapeutic agents. For instance, LCO-1 exhibited no sensitivity to all four reagents, as indicated by relative cell survival. In contrast, LCO-2 demonstrated high sensitivity specifically towards doxorubicin and erlotinib, but displayed resistance to cisplatin and paclitaxel due to its unaffected viability upon treatment with cisplatin and paclitaxel. Additionally, LCO-3 showed sensitivity to doxorubicin, erlotinib and paclitaxel, without any response observed towards cisplatin (Fig. 6b). These findings emphasize the necessity of
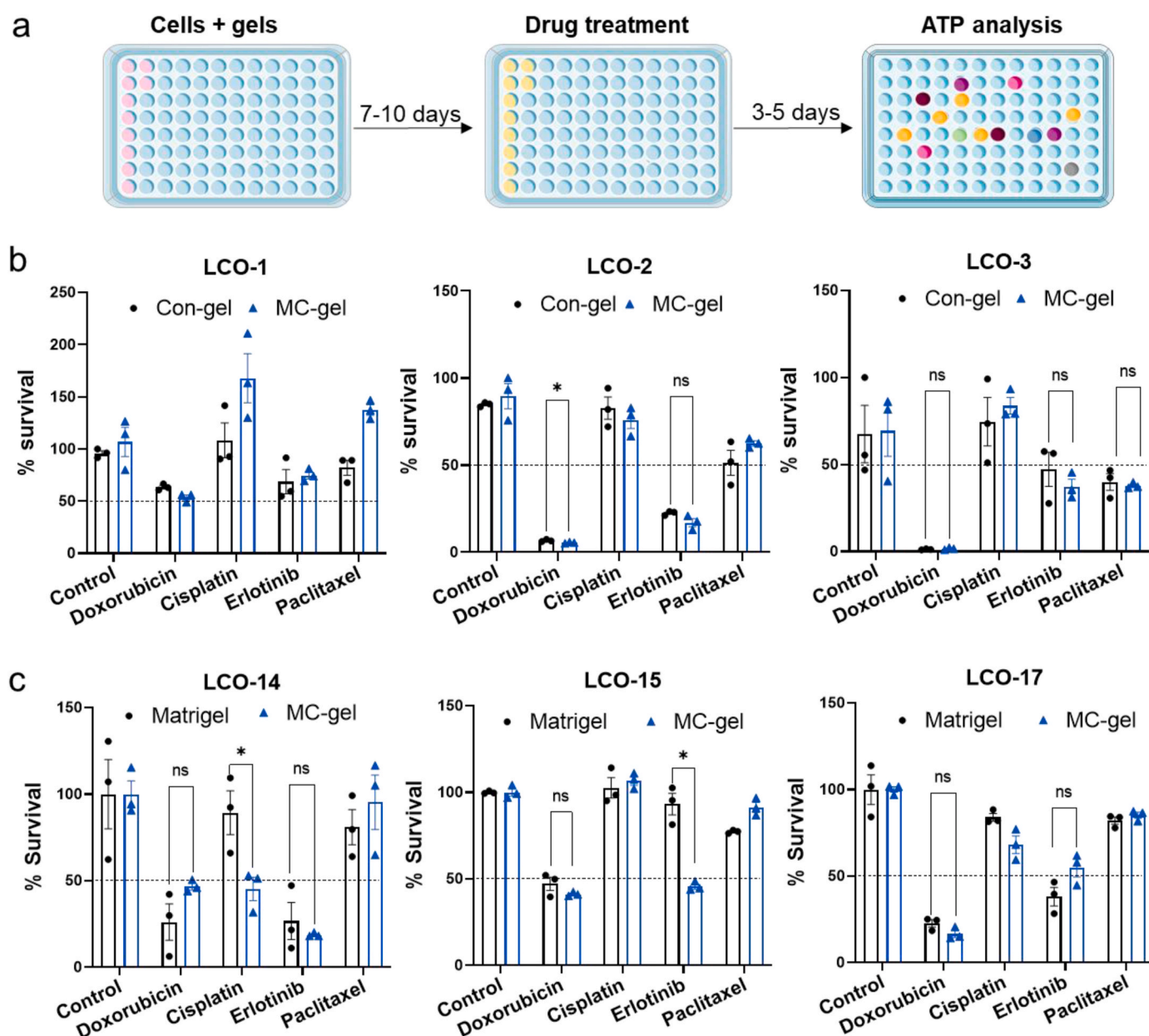
Fig. 6. Drug testing of organoids in the Con-gel and MC-gel. (a) The flow chart illustrating the process of drug testing. (b) Three LCOs cultivated on Con-gel and MC-gel were exposed to doxorubicin, cisplatin, erlotinib, and paclitaxel; the survival was then evaluated by measuring the relative cell survival. (c) The survival of three LCOs cultivated on Matrigel and MC-gel was assessed after exposure to the aforementioned four anti-cancer drugs, by measuring their relative cell survival. The data in (b–c) were presented as the mean ± standard deviation (n = 3). *p < 0.05.

rapid *in vitro* drug sensitivity testing for determining the optimal chemotherapy regimen for individual patients.

Meanwhile, to evaluate the individualized responses to cancer therapies in MC-gel and Matrigel, we also conducted drug sensitivity tests on LCOs cultured in MC-gel and existing models Matrigel. It was observed that LCOs in both matrices exhibited a similar trend (Fig. 6c). However, it is worth noting that LCO-14 cultured in MC-gel demonstrated sensitivity to cisplatin, whereas those cultured in Matrigel did not exhibit a similar trend. Additionally, LCO-15 cultured in MC-gel showed sensitivity to erlotinib, while LCO-15 cultured in Matrigel displayed resistance to erlotinib (Fig. 6c). These findings suggest that LCOs cultured in the MC-gel demonstrate increased susceptibility to these two drugs, potentially due to disparities in growth states between the two hydrogels.

2.7. The MC-gel enables the establishment of long-term cultures of LCOs

Out of the 18 LCOs tested, a remarkable four managed to establish long-term cultures, resulting in a success rate of 22 %. The MC-gel cultured organoid models demonstrated the ability to establish long-term cultures, characterized by sustained cell growth with consistent split ratios even in late passages (9/10 passages, Fig. 7a and b). These cultures could be successfully propagated for over three months with a minimum splitting ratio of 1:2, without experiencing a significant decline in their proliferative abilities as the passages progressed (Fig. 7a and b). Furthermore, they exhibited viability after cryopreservation for more than three months and were capable of expansion upon thawing. In addition, the long-term established lung cancer organoids (LCOs) in MC-gel also exhibited sustained drug sensitivity characteristics similar to their short-term counterparts (Fig. 7c), thereby highlighting the potential of utilizing these long-term established LCOs for personalized treatment strategies in lung cancer patients.

3. Discussion

The three-dimensional (3D) culture models *in vitro* provide a more precise replication of the intricate interactions observed between cell-ECM or between cell-cell *in vivo* [44,45]. Here, we have successfully formulated a novel biomimetic hydrogel composed of mTGase gelatin and natural collagen bundles to effectively initiate and expand LCOs. The unique architecture and mechanical properties of these mesoscale collagen bundles provide an exact representation of the mechanical landscape, enabling optimal conditions for cellular cultivation.

To obtain tumor organoids from patients, the tumor tissues were dissociated into a single cell suspension along with extracellular matrix (ECM) debris (Fig. 2a). Most recent studies have primarily focused on cultivating tumor organoids solely from patient-derived tumor cells, neglecting the importance of ECM debris. In our organoid culture system, we utilized both tumor cells and ECM fragments derived from the tumor tissues to cultivate tumor organoids that retain the essential components of the original tissue at their highest level. The ECM fragments obtained from the tumor tissue consist predominantly of collagen (Fig. 1c), which exhibits a distinct mesoscale architecture within its structure. Furtherly, we present a method for modulation of the collagen derived from the digested debris of patient tumor tissue by mechanical abrasion. With this approach, we have generated collagen-rich scaffolds, which are thickening on a large scale, while retaining global architecture.

The pore structure, physicochemical properties, mechanical behavior, and swelling characteristics of MC-gel were investigated. It was observed that the MC-gel exhibited significantly larger pore dimensions compared to Con-gel. This phenomenon can be attributed to a decline in the level of crosslinking caused by disruption from collagen bundles at the mesoscale. Furthermore, the inclusion of mesoscale collagen bundles is anticipated to bolster the structural soundness of the hydrogel framework, thereby diminishing contraction of pore structures during freeze-drying. There was a slightly reduced storage modulus for MC-gel, compared to Con-gel. Furthermore, FTIR results showed that the chemical composition of mesoscale collagen bundles was identical to that of gelatin. Finally, The MC-gel exhibits a slight decrease in swelling, possibly due to the anti-swelling behavior provided by the mesoscale collagen fibers. All these factors contribute to effectively replicating the tumor microenvironment in patients.

Compared to the existing Matrigel model, MC-gel provides a more individualized approach by utilizing collagen bundle components sourced directly from patients, in contrast to Matrigel from sarcoma cells of the Engelbreth-Holm-Swarm mouse [6], this indicates that MC-gel is better suited for personalized patient treatment. Moreover, the Young's modulus of MC-gel is 12.56 ± 2.7 kPa (Fig. 1k), which closely aligns with the Young's modulus of lung tumor tissue (12.73 kPa) [42], while Matrigel typically exhibits a Young's modulus of approximately 1.29 kPa [46]. Furthermore, MC-gel is designed to replicate the intricate collagen architecture of the tumor extracellular matrix, which has a significant impact on modulating cellular phenotype, mechano-transduction, growth factor communication, intercellular interaction over long distances, and cancer cell infiltration [32,33]. Consequently, tumor organoids with mesoscale architecture exhibit significantly larger diameters and irregular shapes compared to those cultured in Matrigel (Fig. 2b and c).

Furthermore, these specific bundles of collagen can readily be integrated into the co-culture system, encompassing various biodegradable protein-derived hydrogels (such as Matrigel, collagen, or gelatin). We utilized mTG cross-linking gelatin as a platform for incorporating mesoscale collagen bundles due to its non-toxic, non-carcinogenic, biocompatible, and biodegradable properties [27,28]. Moreover, gelatin exhibits low antigenicity as it is denatured unlike collagen which has high antigenicity owing to its animal origin. Importantly, mTG cross-linking gelatin provides the arginine-glycine-aspartate (RGD) motif that induces "outside-in" signaling resulting in intracellular phosphorylation, cytoskeleton reorganization, and granule secretion [23,47,48].

The advantages of both collagen bundles and mTG cross-linking gelatin are combined in this model for the purpose of culturing tumor organoids from patients. Gelatin promotes cell-matrix interactions by providing the RGD integrin receptor binding motif that is present in natural extracellular matrix proteins. The formation of mesoscale collagen bundles results in a natural architecture of MC-gel, providing a distinct scaffold for cellular activities and intercellular communication. This emphasizes the significance of the unique architecture formed by mesoscale collagen within the microenvironment surrounding tumors. However, the limited availability of mesoscale collagen bundles obtained from the patients is attributed to the size of cancer tissue and the efficiency of digestion. It is crucial to optimize the balance between the quantity of cancer cells and mesoscale collagen bundles in order to achieve optimal outcomes.

PDTO possess the capability to facilitate the advancement of personalized therapeutic approaches for cancer patients [16,22,49,50]. In our investigations, lung cancer organoids cultured in MC-gel accurately recapitulate the histological characteristics and mutational profile of the original tumor from the donor patient. Furthermore, we have demonstrated that the presence of mesoscale collagen bundles insignificantly influences gene expression and drug response in these organoids. Owing to faithfully recapitulating the original tumor's features, MC-gel offers a valuable opportunity to serve as a scaffold for comprehending individual drug reactions and tailoring treatments according to patients' distinct molecular and clinical characteristics. Meanwhile, the MC-gel can be utilized for extended culture periods, facilitating sustained growth of LCOs and preserving their drug sensitivity. Beside LCOs studied in our research, tumor organoids derived from other organs also are established using MC-gel model. The MC-gel possesses the potential for extensive utilization in the domains of wound healing, tumor metastasis, and 3D stem cell differentiation. Our findings indicate that
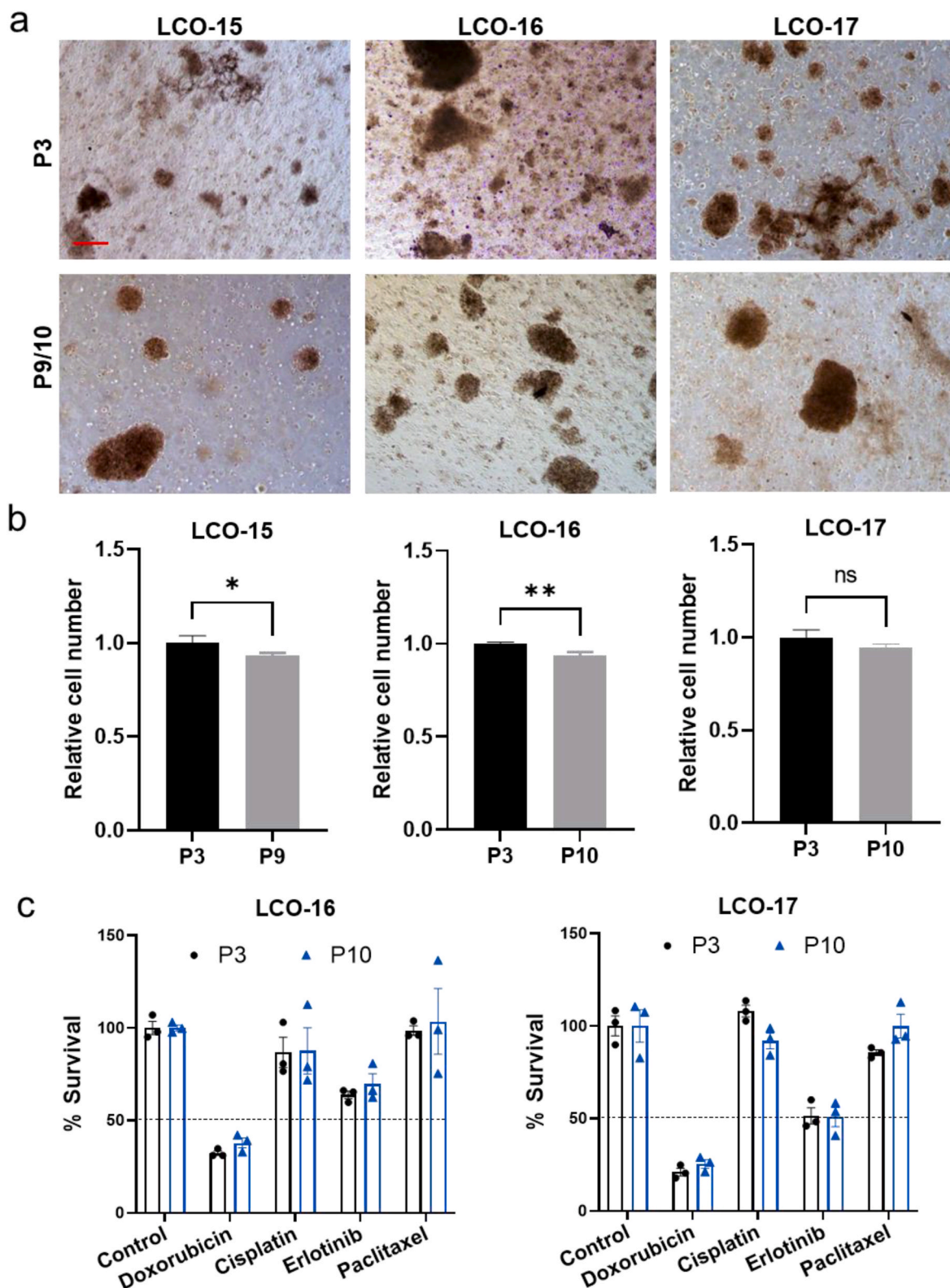
Fig. 7. Growth characterization and drug testing of long-term organoid in MC-gel. (a–b) Representative micrographs in bright-field of LCOs subjected to an extended period (P9/10) and a shorter duration (P3) in MC-gel were presented, and their numbers were quantified. Scale bar, 200 μm. (c) The viability of two long-term cultured LCOs (P9/10) and one short-term cultured LCO (P3) in MC-gel was evaluated following exposure to the aforementioned four anti-cancer drugs, through assessment of their relative cell survival. Data in (c) were plotted as mean ± standard deviation (n = 3). *p < 0.05. **p < 0.01.

the MC-gel model has the potential to replicate patient outcomes in a clinical setting and can be effectively incorporated into a personalized medicine initiative.

4. Methods

4.1. Tumor specimen collection

Samples (1–2.5 cm^3) of lung cancer (LC), sarcoma and thyroid cancer were collected from the Cancer Hospital & Shenzhen Hospital, Chinese Academy of Medical Sciences and promptly transported to the laboratory following surgery. Supplementary Table 1 listed the clinical characteristics of patient donors with lung cancer. The sarcoma sample was acquired from a 51-year-old male patient diagnosed with fibrosarcoma, whereas a female patient aged 35 years contributed to the collection by providing a sample originating from her thyroid cancer. The collection of human samples for this study was granted full ethical approval by the Ethics Committee of Cancer Hospital & Shenzhen Hospital, Chinese Academy of Medical Sciences (KYLX2023-106). Additionally, all patients provided written informed consent for the utilization of surgically obtained tissue.

4.2. Mesoscale collagen bundle preparation

The tumor samples were washed twice with cold PBS prior to being minced into 1–2.5 mm^3 fragments using scissors. The minced tissue was subsequently incubated with 5 ml of collagenaseI (3 mg/ml) and a ROCK inhibitor, Y-27632 dihydrochloride (10 μM), in a 15 ml centrifuge tube for 1.5 h using a constant temperature culture shaker (WS20, Shanghai) set at 50 rpm and maintained at 37 °C until the observation of significant amounts of flocculent precipitate and cell suspensions. Following digestion, the tissue samples were passed through a cell strainer (70 μM) to segregate large undigested clusters from single-cell suspensions. The large undigested clusters were subsequently subjected multiple freeze-thaw cycles at −80 °C and room temperature to eliminate the remaining cells. Subsequently, the left fibers were homogenized at 4 °C using a tissue grinder (Fish Scientific) operating at a speed of 6.5 m/s. The homogenization process involved shaking for 1 min, followed by a 1-min hold period, and repeated for a total of 7 cycles. This resulted in the generation of medium-sized collagen bundles measuring approximately 90 ± 27 μm in length and having an average diameter ranging from 3.5 to 6.5 μm. The medium-sized collagen fibers are subsequently sterilized and inactivated by immersing them in 75 % alcohol for 1 h, followed by thorough washing with sterile deionized water (4–5 times) for preservation.

4.3. MC-gel preparation

To prepare the MC-gel hydrogel, we measured and dissolved type A 300 Bloom gelatin powder (Sigma-Aldrich, MO, USA) in sterile deionized water at a temperature of 50 °C. Subsequently, we rapidly sterilized the solution using a 0.22 mm filter to avoid any blockage resulting from the cooling gel. Different concentrations of mesoscale collagen bundles were incorporated into the 4 % gelatin solutions, followed by the addition of mTG derived from Streptoverticillium mobaraense by Ajinomoto Corporation Inc., Japan, to the gelatin/collagen bundles prior to their use in organoid culture. The transglutaminases used in this investigation had a typical activity level of 20,000 U/mg. The Nano-gel was prepared by mixing 4 % gelatin with 1 mg/ml type I collagen, (Corning 354249). The Matrigel (Corning, 356255) was purchased from the company.

4.4. Digestion of MC-gel

The Con-gel and MC-gel were fragmented into smaller clusters through trituration using 1 ml pipette tips, followed by subsequent digestion with type IV collagenase (2 mg/ml) or TE solution (Gibco) until complete dissolution of all gels was achieved. The duration of digestion was recorded.

4.5. Elastic modulus measurement

Nanoindentation tests were conducted using a displacement-controlled PIUMA Nanoindenter (Optics11, Amsterdam, The Netherlands) according to the manufacturer's instructions. Briefly, mTGase cross-linked gelatin with different concentrations of mesoscale collagen bundles were affixed onto a glass-bottom dish using Pattex glue. Spherical tips with radii of 50 μm ($k = 0.5$ N/m) were utilized for sample testing. The calibration of cantilever bending was conducted prior to each set of experiments by applying pressure on a solid surface and establishing an equivalence between cantilever bending and probe displacement. Following calibration, the dish with the sample was set on the PIUMA sample stage. The samples were immersed in PBS at room temperature, ensuring that the nanoindenter tip remained well below the solution surface throughout the process to prevent errors caused by strong adhesive forces at the air-water interface. The stress-testing of each sample was conducted 5–6 times, ensuring a minimum distance of 200 μm between measurements. The effective Young's modulus of each sample was calculated from multiple measurements. At least four independent test per group were used for quantification purposes.

4.6. Rheometry

The rheological properties were evaluated using the HR20 rotary rheometer from TA Instruments (USA). This device features a precision-engineered 20 mm diameter testing platform and a gap size of 500 μm. After allowing for a heat equilibrium time of 180s, the temperature of the system was set at a constant value of 25 °C throughout the experiment. The applied strain in the strain scanning experiments varied from 0.1 % to 100 %. In the frequency sweep experiment, a constant strain value of 1 % was maintained while varying the frequency from 0.1 to 100 %. Finally, in the stress relaxation experiment, a fixed strain setting of 2 % was used with a total test time of 600s.

4.7. Scanning electron microscopy (SEM)

The MC-gel and Con-gel were prepared and flash-frozen in liquid nitrogen for 10 min. Subsequently, they were subjected to freeze-drying for 24 h under a pressure of 2 Pa to preserve the integrity of their porous structure. The freeze-dried samples were carefully cut using a surgical knife and affixed onto aluminum holders. Subsequently, a layer of gold was applied to the samples through sputter-coating prior to imaging their porous morphologies by a SEM (HITACHI, Regulus 8100) operating at an acceleration voltage of 20 kV and an initial magnification of $100 \times$. For pore diameter measurement, more than 100 pores per group were quantified.

4.8. Fourier-transform infrared spectroscopy (FTIR)

The Fourier-transform infrared spectroscopy (FTIR) analysis was performed using a VERTEX70 infrared spectrometer (Bruker, Germany) under reflected ATR mode to examine the freeze-dried hydrogel samples within the spectra range of 400–4000 cm^{-1}, enabling the acquisition of microscopic information regarding chemical functional group composition.

4.9. Swelling

MC-gels and Con-gels were accurately weighed and subsequently submerged in an excess of distilled water at room temperature for incubation periods of 0, 2, 6, 12, and 24 h. Following this, the swollen hydrogels were delicately removed using tweezers, gently wiped with a

filter paper to eliminate any surface moisture, and re-weighed. The repetition of the process continued until achieving consistent weights. The swelling ratio was determined by calculating the average of three values using the provided equation. Swelling ratio = (Wb - Wa)/Wa × 100 %. Herein, Wb represents the weight of the wet scaffold while Wa denotes the weight of the dry scaffold.

4.10. Organoid culture

The suspension of cells obtained from the methods described in the "Mesoscale collagen bundle preparation" section was centrifuged at 1000 g for 5 min, followed by a PBS wash and another round of centrifugation at 1000g for a duration of 5 min. Finally, the tumor cells were re-suspended in a gelatin solution containing a concentration of 4 %. Ten drops of a mixture consisting of MC-gel (~20 μL) and cells (~20,000 cells/drop) were plated into each well of a six-well plate. They were carefully incubated in a 37 °C atmosphere with a 5 % CO2 concentration for further incubation. Once solidified, each well received an addition of Lung cancer organoid medium (2 ml).

The lung cancer organoid medium used in this study was prepared by combining Advanced DMEM/F12 medium with B27 supplement (17504044, Gibco), penicillin/streptomycin (C0222, Beyotime), Primocin solution (1 mg/mL) (ant-pm-1, InvivoGen), N-acetyl-ʟ-cysteine compound (1 mM, HY-B0215, MCE), recombinant Noggin protein solution (0.1 μg/mL,Z03212,Gene script), epidermal growth factor EGF (50 ng/mL,Z00333,Gene script), fibroblast growth factor FGF (40 ng/mL,Z03116, Genescript), Nicotinamide compound (10 mM,HY-B0150, MCE), SB202190 compound (10 μM,HY-10295,MCE) and A83-01 compound (0.5 μM,HY-10432,MCE). The culture media were refreshed every three days while freshly-prepared media were used on a weekly basis.

For passaging, the MC-gel drops were harvested from the plate and fragmented into smaller pieces using a cell scalpel, followed by a centrifugation step at 1000 g for 3 min. The cell pellet and the MC-gel were digested with collagenase IV (2 mg/ml) containing Y-27632 dihydrochloride (10 μM) for approximately 5–10 min at 37 °C. Organoids were then centrifuged at 200 g for 5 min, washed once with culture medium, and centrifuged again. Organoids were cultured for a duration of approximately two to three weeks. Subsequently, organoids were passaged at a ratio ranging from one to two to one to three every two to three weeks. To preserve them, the organoids were separated from the MC-gel and subsequently cryopreserved using cell freezing medium supplemented with Y-27632 dihydrochloride (10 μM).

4.11. H&E staining and IF analysis

The fresh lung tumor tissue was initially immersed in a 10 % formalin solution for a period ranging from 24 to 48 h, then transfer to a 70 % ethanol solution for further preservation before being embedded in paraffin. The organoids cultured in MC-gel and Con-gel were immersed in a 4 % formalin solution for a duration of 24–48 h and then treated with eosin in a 70 % ethanol solution prior to embedding them in agarose (2 %) for subsequent processing involving H&E staining and immunofluorescence (IF) analysis. The tumor tissues and organoids, which had been embedded in paraffin, were sliced into sections with an approximate thickness of 4 μm and left to dry overnight at a temperature of 60 °C. For immunofluorescence experiments, paraffin slides underwent antigen retrieval by employing a citric acid solution (pH 6.0) after deparaffinization and rehydration. The prepared tissue sections were subjected to appropriate antibody staining using the primary antibodies Napsin A (ABclonal, A5594), Cytokeratin5/6 (CK5/6) (Proteintech, 28506-1-AP), TP63 (Proteintech, 12143-1-AP), TTF-1 (ABclonal, A18128), Cytokeratin 7(CK7, Proteintech, 17513-1-AP), Ki67 (Proteintech, 27309-1-AP). The slides were then rinsed with PBS and subjected to incubation with diluted secondary antibodies for 1 h at 25 °C. The nuclei were labeled with DAPI. Subsequently, the slides were

scanned and captured using a confocal microscope manufactured by Leica (LSM900).

4.12. DNA extraction and analysis of whole exome sequencing (WES)

The QIAamp DNA FFPE Tissue Kit (QIAGEN, 56404) was utilized for the extraction of total DNA, followed by fragmentation using the Covaris M220 Focused-ultrasonicator and subsequent preparation for sequencing library construction. The Human Exome 2.0 Plus kit (Twist Bioscience) was utilized for exome capture, according to manufacturer's protocol provided by the vendor. The Illumina NovaSeq 6000 Sequencing System (Illumina) was conducted for paired-end 150 bp sequencing of the final libraries at LC-Bio Technology Co., Ltd (Hangzhou, China). Prior to alignment, fastp software was employed to eliminate low quality reads containing sequencing adaptors or nucleotides with q quality20 [51]. For alignment purposes, we employed BWA (Burrows Wheeler Aligner) [52] to align reads against the hg19 reference genome. Post-alignment processing involved duplicate read identification and marking using Picard tools from Broad Institute's repository website. Additionally, a secondary post-alignment processing step was conducted to address potential alignment errors near indels by implementing local read realignment. To mitigate systematic biases prior to variant calling, recalibration of base quality scores was conducted. The somatic SNVs and InDels were detected through the combined utilization of Mutect2 algorithm [53] while ANNOVAR incorporated biological information into the set of variants [54]. Copy number variations were detected using CNVkit software toolset [55]. Normalization of read distribution based on GC content of sequences facilitated calculation of copy number differences between tumor and normal samples.

4.13. RNA sequencing

The Trizol reagent (thermofisher, 15596018) was employed to extract the total RNA in following the manufacturer's guidelines. Subsequently, we assessed the quantity and purity of the isolated RNA using Bioanalyzer 2100 Nano LabChip Kit (Agilent, 5067-1511). For constructing the sequencing library, only high-quality RNA samples with an RIN number exceeding 70 were utilized. To isolate mRNA from a 5ug portion of total RNA, two purification cycles were performed by Dynabeads Oligo (dT) (Thermo Fisher, 61005). The purified mRNA was subsequently subjected to fragmentation at 94 °C for 5–7 min using divalent cations (NEB, e6150). The fragmented RNA was converted into complementary DNA through cDNA synthesis using SuperScript™ II Reverse Transcriptase (Invitrogen, 1896649). Next, DNA polymerase I (NEB, m0209), RNase H (NEB, m0297), and dUTP Solution (Thermo Fisher, R0133) were employed to synthesize U-labeled second-stranded DNAs from the cDNA templates. In order to facilitate ligation of indexed adapters, an A-base was introduced at the blunt ends of each strand. The adapters themselves had a T-base overhang, which aided in the ligation process with A-tailed fragmented DNA molecules. Subsequently, these fragments underwent dual-index adapter ligation and size selection using AMPureXP beads. Following treatment with heat-labile UDG enzyme (NEB, m0280), PCR amplification was performed on these fragments after dual-index adapter ligation. The average size of the inserted fragments in the ultimate cDNA libraries varied within the range of 300 ± 50 bp. Subsequently, we utilized the Illumina Novaseq™6000 (LC-Bio Technology CO., Ltd., Hangzhou China) for conducting paired-end sequencing (PE150) with read lengths of 2 × 150 bp, following the vendor's suggested procedure.

We utilized R for conducting correlation analysis, which enables us to evaluate the reliability and operational stability of experimental results through the correlation of parallel experiments of organoids in MC-gel and Con-gel. To evaluate the consistency among samples, we computed the Pearson correlation coefficient between four pairs of organoids in MC-gel and Con-gel. A higher correlation coefficient

indicates a greater degree of reproducibility observed in these parallel experiments. For this specific study, we utilized the princomp function in R (http://www.r-project.org/) for conducting principal component analysis (PCA).

4.14. In vitro drug studies

The compounds used for conducting drug testing in a laboratory setting, as described in Table S2, were obtained from MedChemExpress and dissolved either in dimethyl sulfoxide (DMSO) or PBS following the provided guidelines. The organoids were dissociated into individual cells, quantified, and then seeded in black 96-well plates with triplicate wells containing 10,000 cells per well. These plates were incubated for a growth period of 7–10 days. The organoids were subsequently exposed to drug concentrations of 10 μmol/L for a duration of 3–5 days. Afterward, cell viability was assessed by employing the CellTiter-Lumi™ Luminescent Assay Kit for evaluating the viability of three-dimensional (3D) cells (Beyotime, C0061S), following the instructions provided by the manufacturer. To standardize variability across different plates during data analysis, we calculated the control percentage. The signal obtained from wells treated with DMSO alone served as our negative control and was set at 0 %, while wells without any drug treatment were assigned a value of 100 % on each individual plate. Relative cell survival was determined based on three biological replicates.

4.15. Statistical analysis

The mean $\pm$ standard deviation (SD) was used to present the experimental data. Statistical analysis was conducted using GraphPad Prism Software Version 9.5 (GraphPad Software Inc, USA) or Origin (OriginLab Corp., USA). Student's *t*-test was employed for comparing two groups, while one-way ANOVA analysis with Tukey's post hoc tests was utilized for comparisons among three or more groups. A significance level of *p $<$ 0.05 was considered statistically significant.

Ethics approval and consent to participate

The collection of human samples for this study was granted full ethical approval by the Ethics Committee of Cancer Hospital & Shenzhen Hospital, Chinese Academy of Medical Sciences (KYLX2023-106). Additionally, all patients provided written informed consent for the utilization of surgically obtained tissue.

CRediT authorship contribution statement

Jiaxin Wang: Writing – original draft, Methodology, Investigation, Data curation. **Zhilin Sui:** Methodology, Investigation, Data curation. **Wei Huang:** Methodology, Investigation. **Zhentao Yu:** Writing – review & editing, Supervision, Funding acquisition. **Ling Guo:** Writing – review & editing, Supervision, Project administration, Funding acquisition, Conceptualization.

Declaration of competing interest

The authors declare that none of them have any conflict of interest.

Acknowledgments

Appendix A. Supplementary data

Supplementary data to this article can be found online at https://doi.org/10.1016/j.bioactmat.2024.04.035.

References

[1] S.-Y. Kim, S.-M. Kim, S. Lim, J.Y. Lee, S.-J. Choi, S.-D. Yang, M.R. Yun, C.G. Kim, S. R. Gu, C. Park, et al., Modeling clinical responses to targeted therapies by patient-derived organoids of advanced lung adenocarcinoma, Clin. Cancer Res. 27 (15) (2021) 4397–4409.

[2] R. Shi, N. Radulovich, C. Ng, N. Liu, H. Notsuda, M. Cabanero, S.N. Martins-Filho, V. Raghavan, Q. Li, A.S. Mer, et al., Organoid cultures as preclinical models of non–small cell lung cancer, Clin. Cancer Res. 26 (5) (2020) 1162–1174.

[3] G. Vlachogiannis, S. Hedayat, A. Vatsiou, Y. Jamin, J. Fernandez-Mateos, K. Khan, A. Lampis, K. Eason, I. Huntingford, R. Burke, et al., Patient-derived organoids model treatment response of metastatic gastrointestinal cancers, Science 359 (6378) (2018) 920–926.

[4] D. Tuveson, H. Clevers, Cancer modeling meets human organoid technology, Science 364 (6444) (2019) 952–955.

[5] M. Kim, H. Mun, C.O. Sung, E.J. Cho, H.-J. Jeon, S.-M. Chun, D.J. Jung, T.H. Shin, G.S. Jeong, D.K. Kim, et al., Patient-derived lung cancer organoids as *in vitro* cancer models for therapeutic screening, Nat. Commun. 10 (1) (2019) 3991.

[6] E. Prince, J. Cruickshank, W. Ba-Alawi, K. Hodgson, J. Haight, C. Tobin, A. Wakeman, A. Avoulov, V. Topolskaia, M.J. Elliott, et al., Biomimetic hydrogel supports initiation and growth of patient-derived breast tumor organoids, Nat. Commun. 13 (1) (2022) 1466.

[7] F. Jacob, R.D. Salinas, D.Y. Zhang, P.T.T. Nguyen, J.G. Schnoll, S.Z.H. Wong, R. Thokala, S. Sheikh, D. Saxena, S. Prokop, et al., A patient-derived glioblastoma organoid model and biobank recapitulates inter- and intra-tumoral heterogeneity, Cell 180 (1) (2020) 188–204 e122.

[8] M. Bleijs, M. van de Wetering, H. Clevers, J. Drost, Xenograft and organoid model systems in cancer research, EMBO J. 38 (15) (2019) e101654.

[9] G.J. Yoshida, Applications of patient-derived tumor xenograft models and tumor organoids, J. Hematol. Oncol. 13 (1) (2020) 4.

[10] H.F. Farin, M.H. Mosa, B. Ndreshkjana, B.M. Grebbin, B. Ritter, C. Menche, K. B. Kennel, P.K. Ziegler, L. Szabo, J. Bollrath, et al., Colorectal cancer organoid-stroma biobank allows subtype-specific assessment of individualized therapy responses, Cancer Discov. 13 (10) (2023) 2192–2211.

[11] S. Mo, P. Tang, W. Luo, L. Zhang, Y. Li, X. Hu, X. Ma, Y. Chen, Y. Bao, X. He, et al., Patient-derived organoids from colorectal cancer with paired liver metastasis reveal tumor heterogeneity and predict response to chemotherapy, Adv. Sci. 9 (31) (2022) e2204097.

[12] L. Huang, A. Holtzinger, I. Jagan, M. BeGora, I. Lohse, N. Ngai, C. Nostro, R. Wang, L.B. Muthuswamy, H.C. Crawford, et al., Ductal pancreatic cancer modeling and drug screening using human pluripotent stem cell– and patient-derived tumor organoids, Nat. Med. 21 (11) (2015) 1364–1371.

[13] B.T. Grünwald, A. Devisme, G. Andrieux, F. Vyas, K. Aliar, C.W. McCloskey, A. Macklin, G.H. Jang, R. Denroche, J.M. Romero, et al., Spatially confined sub-tumor microenvironments in pancreatic cancer, Cell 184 (22) (2021) 5577–5592. e5518.

[14] S.J. Hill, B. Decker, E.A. Roberts, N.S. Horowitz, M.G. Muto, M.J. Worley, C. M. Feltmate, M.R. Nucci, E.M. Swisher, H. Nguyen, et al., Prediction of DNA repair inhibitor response in short-term patient-derived ovarian cancer organoids, Cancer Discov. 8 (11) (2018) 1404–1421.

[15] S. Karkampouna, F. La Manna, A. Benjak, M. Kiener, M. De Menna, E. Zoni, J. Grosjean, I. Klima, A. Garofoli, M. Bolis, et al., Patient-derived xenografts and organoids model therapy response in prostate cancer, Nat. Commun. 12 (1) (2021) 1117.

[16] P. Chen, X. Zhang, R. Ding, L. Yang, X. Lyu, J. Zeng, J.H. Lei, L. Wang, J. Bi, N. Shao, et al., Patient-derived organoids can guide personalized-therapies for patients with advanced breast cancer, Adv. Sci. 8 (22) (2021) e2101176.

[17] S. Bhatia, M. Kramer, S. Russo, P. Naik, G. Arun, K. Brophy, P. Andrews, C. Fan, C. M. Perou, J. Preall, et al., Patient-derived triple-negative breast cancer organoids provide robust model systems that recapitulate tumor intrinsic characteristics, Cancer Res. 82 (7) (2022) 1174–1192.

[18] G. Vlachogiannis, S. Hedayat, A. Vatsiou, Y. Jamin, J. Fernández-Mateos, K. Khan, A. Lampis, K. Eason, I. Huntingford, R. Burke, et al., Patient-derived organoids model treatment response of metastatic gastrointestinal cancers, Science 359 (6378) (2018) 920–926.

[19] P. Sikdar, M.M. Uddin, T.M. Dip, S. Islam, M.S. Hoque, A.K. Dhar, S. Wu, Recent advances in the synthesis of smart hydrogels, Mater. Adv. 2 (14) (2021) 4532–4573.

[20] A. Bordbar-Khiabani, M. Gasik, Smart hydrogels for advanced drug delivery systems, Int. J. Mol. Sci. 23 (7) (2022) 3665.

[21] A. Raza, C.S. Ki, C.C. Lin, The influence of matrix properties on growth and morphogenesis of human pancreatic ductal epithelial cells in 3D, Biomaterials 34 (21) (2013) 5117–5127.

[22] H. Dong, Z. Li, S. Bian, G. Song, W. Song, M. Zhang, H. Xie, S. Zheng, X. Yang, T. Li, et al., Culture of patient-derived multicellular clusters in suspended hydrogel capsules for pre-clinical personalized drug screening, Bioact. Mater. 18 (2022) 164–177.

[23] Y. Zhou, S. Liao, Y. Chu, B. Yuan, X. Tao, X. Hu, Y. Wang, An injectable bioink with rapid prototyping in the air and in-situ mild polymerization for 3D bioprinting, Biofabrication 13 (4) (2021) 045026.

[24] D.Y.S. Chau, R.J. Collighan, E.A.M. Verderio, V.L. Addy, M. Griffin, The cellular response to transglutaminase-cross-linked collagen, Biomaterials 26 (33) (2005) 6518–6529.

[25] Y. Liu, R. Weng, W. Wang, X. Wei, J. Li, X. Chen, Y. Liu, F. Lu, Y. Li, Tunable physical and mechanical properties of gelatin hydrogel after transglutaminase crosslinking on two gelatin types, Int. J. Biol. Macromol. 162 (2020) 405–413.

[26] C.C. Tsai, Y.J. Hong, R.J. Lee, N.C. Cheng, J. Yu, Enhancement of human adipose-derived stem cell spheroid differentiation in an in situ enzyme-crosslinked gelatin hydrogel, J. Mater. Chem. B 7 (7) (2019) 1064–1075.

[27] C.C. Tu, N.C. Cheng, J. Yu, Y.X. Pan, W.C. Tai, Y.C. Chen, P.C. Chang, Adipose-derived stem cell spheroid-laden microbial transglutaminase cross-linked gelatin hydrogel for treating diabetic periodontal wounds and craniofacial defects, Stem Cell Res. Ther. 14 (1) (2023) 20.

[28] G. Yang, Z. Xiao, X. Ren, H. Long, H. Qian, K. Ma, Y. Guo, Enzymatically crosslinked gelatin hydrogel promotes the proliferation of adipose tissue-derived stromal cells, PeerJ 4 (2016) e2497.

[29] H.T. Nia, L.L. Munn, R.K. Jain, Physical traits of cancer, Science 370 (6516) (2020) eaaz0868.

[30] P.P. Provenzano, K.W. Eliceiri, J.M. Campbell, D.R. Inman, J.G. White, P.J. Keely, Collagen reorganization at the tumor-stromal interface facilitates local invasion, BMC Med. 4 (1) (2006) 38.

[31] M.W. Conklin, J.C. Eickhoff, K.M. Riching, C.A. Pehlke, K.W. Eliceiri, P.P. Provenzano, A. Friedl, P.J. Keely, Aligned collagen is a prognostic signature for survival in human breast carcinoma, Am. J. Pathol. 178 (3) (2011) 1221–1232.

[32] X. Gong, J. Kulwatno, K.L. Mills, Rapid fabrication of collagen bundles mimicking tumor-associated collagen architectures, Acta Biomater. 108 (2020) 128–141.

[33] C. Liu, R.Y. Nguyen, G.A. Pizzurro, X. Zhang, X. Gong, A.R. Martinez, M. Mak, Self-assembly of mesoscale collagen architectures and applications in 3D cell migration, Acta Biomater. 155 (2023) 167–181.

[34] M.W. Conklin, P.J. Keely, Why the stroma matters in breast cancer, Cell Adhes. Migrat. 6 (3) (2014) 249–260.

[35] F. Kai, A.P. Drain, V.M. Weaver, The extracellular matrix modulates the metastatic journey, Dev. Cell 49 (3) (2019) 332–346.

[36] K.B. Pointer, P.A. Clark, A.B. Schroeder, M.S. Salamat, K.W. Eliceiri, J.S. Kuo, Association of collagen architecture with glioblastoma patient survival, J. Neurosurg. 126 (6) (2016) 1812–1821.

[37] J. Sievers, V. Mahajan, P.B. Welzel, C. Werner, A. Taubenberger, Precision hydrogels for the study of cancer cell mechanobiology, Adv. Healthcare Mater. 12 (14) (2023) e2202514.

[38] A. Cambi, M. Ventre, Collagen-based biomimetic systems to study the biophysical tumour microenvironment, Cancers 14 (23) (2022) 5939.

[39] M. Kim, M. Panagiotakopoulou, C. Chen, S.B. Ruiz, K. Ganesh, T. Tammela, D.A. Heller, Micro-engineering and nano-engineering approaches to investigate tumour ecosystems, Nat. Rev. Cancer 23 (9) (2023) 581–599.

[40] C. Liu, R.Y. Nguyen, G.A. Pizzurro, X. Zhang, X. Gong, A.R. Martinez, M. Mak, Self-assembly of mesoscale collagen architectures and applications in 3D cell migration, Acta Biomater. 155 (2023) 167–181.

[41] A.J. Berger, K.M. Linsmeier, P.K. Kreeger, K.S. Masters, Decoupling the effects of stiffness and fiber density on cellular behaviors via an interpenetrating network of gelatin-methacrylate and collagen, Biomaterials 141 (2017) 125–135.

[42] B.R. Loshusan, A.M. Shamsil, M.D. Naish, R.V. Patel, M. Qiabi, R. Nayak, R.A. Malthaner, Young's moduli of human lung parenchyma and tumours, J. Oncol. Res. Ther. 9 (1) (2024) 10198.

[43] M. Imielinski, H. Berger Alice, Peter S. Hammerman, B. Hernandez, J. Pugh Trevor, E. Hodis, J. Cho, J. Suh, M. Capelletti, A. Sivachenko, et al., Mapping the hallmarks of lung adenocarcinoma with massively parallel sequencing, Cell 150 (6) (2012) 1107–1120.

[44] L.G. Griffith, M.A. Swartz, Capturing complex 3D tissue physiology *in vitro*, Nat. Rev. Mol. Cell Biol. 7 (3) (2006) 211–224.

[45] D. Loessner, S. Kobel, J.A. Clements, M.P. Lutolf, D.W. Hutmacher, Hydrogel microwell arrays allow the assessment of protease-associated enhancement of cancer cell aggregation and survival, Microarrays 2 (3) (2013) 208–227.

[46] F.M. Lartey, M. Rafat, M. Negahdar, A.V. Malkovskiy, X. Dong, X. Sun, M. Li, T. Doyle, J. Rajadas, E.E. Graves, et al., Dynamic CT imaging of volumetric changes in pulmonary nodules correlates with physical measurements of stiffness, Radiother. Oncol. 122 (2) (2017) 313–318.

[47] R. Augustine, Skin bioprinting: a novel approach for creating artificial skin from synthetic and natural building blocks, Prog. Biomater 7 (2) (2018) 77–92.

[48] N. Davidenko, C.F. Schuster, D.V. Bax, N. Raynal, R.W. Farndale, S.M. Best, R.E. Cameron, Control of crosslinking for tailoring collagen-based scaffolds stability and mechanics, Acta Biomater. 25 (2015) 131–142.

[49] H. Xu, D. Jiao, A. Liu, K. Wu, Tumor organoids: applications in cancer modeling and potentials in precision medicine, J. Hematol. Oncol. 15 (1) (2022) 58.

[50] V. Veninga, E.E. Voest, Tumor organoids: opportunities and challenges to guide precision medicine, Cancer Cell 39 (9) (2021) 1190–1201.

[51] S. Chen, Y. Zhou, Y. Chen, J. Gu, fastp: an ultra-fast all-in-one FASTQ preprocessor, Bioinformatics 34 (17) (2018) i884–i890.

[52] H. Li, R. Durbin, Fast and accurate short read alignment with Burrows–Wheeler transform, Bioinformatics 25 (14) (2009) 1754–1760.

[53] K. Cibulskis, M.S. Lawrence, S.L. Carter, A. Sivachenko, D. Jaffe, C. Sougnez, S. Gabriel, M. Meyerson, E.S. Lander, G. Getz, Sensitive detection of somatic point mutations in impure and heterogeneous cancer samples, Nat. Biotechnol. 31 (3) (2013) 213–219.

[54] K. Wang, M. Li, H. Hakonarson, ANNOVAR: functional annotation of genetic variants from high-throughput sequencing data, Nucleic Acids Res. 38 (16) (2010) e164.

[55] E. Talevich, A.H. Shain, T. Botton, B.C. Bastian, CNVkit: genome-wide copy number detection and visualization from targeted DNA sequencing, PLoS Comput. Biol. 12 (4) (2016) e1004873.